Macro-Micro Multi-Arm Instrument for Single-Port Access Surgery

T.Vandebroek[1], M.Ourak[1], C.Gruijthuijsen[1], A.Javaux[1], J.Legrand[1],
T.Vercauteren[3], S.Ourselin[3], J.Deprest[2], E.Vander Poorten[1]

***Abstract*— Minimally invasive surgery is now a well established field in surgery but continuous efforts are made to reduce invasiveness even further. This paper proposes a novel concept of small-diameter multi-arm instrument for Single-Port Access Surgery. The concept introduces a novel combination of backbone and actuation principles in a macro-micro fashion to achieve an excellent decoupling of the triangulation platform (macro) and of the end-effectors (micro). Concentric tube robots are used for the triangulation platform, while compliant fluidic-actuated bending segments are used as end-effectors. The fluidic actuation is advantageous as it minimally interferes with the triangulation platform. The triangulation platform on the other hand provides a stable base for the end-effectors such that large distal actuation bandwidth can be achieved. A specific embodiment for Spina Bifida repair is developed and proposed. The surgical and technical requirements as well as the mechanical design are presented in details. A first prototype is built and characterization experiments are conducted to evaluate its performance.**

I. INTRODUCTION

A. Background

Minimally Invasive Surgery (MIS) is gradually replacing open surgery, leading to reduced post-operative pain, improved cosmetic outcomes, shorter hospital stay and faster recovery [1]. Unfortunately, each port creates a risk of morbidity from hemorrhage, hernia and internal organ injury. With every additional port multiplying these risks, Single Port Access (SPA) surgery is the next logical step. However, where multi-port laparoscopic interventions are already difficult to perform due to a reduced and decoupled 2D vision, the loss of degrees of freedom (DOFs) and tremor amplification due to long instruments and the fulcrum effect [2], SPA surgery is even more challenging. Collisions between instruments, obstruction between multiple clinicians, poor triangulation of the operating site and a further loss of intuitive motion [1] make its adoption by surgeons difficult. Robotic assistance is regarded as having the potential to address all above-mentioned issues.

Most robotic SPA platforms found in the literature, such as the STRAS [3], MASTER [4], ViaCath [5], IREP [6], the system proposed by Lau & al. [7] or the SAIT [8] are cable-actuated hence suffer from hysteresis and friction. Cable transmission contributes to an inefficient force transmission, lack of responsiveness and low accuracy (e.g. due to stick-slip) [9]. Additionally, these systems have a fairly large outer diameter (OD), between 15 to 30mm, whereas regular MIS instruments which range from 3 to 12 mm in diameter. Another category of robotic SPA platform are miniature in-vivo robots like proposed by Petroni *et. al.* [10] or Lehman *et al.* [11]. Their miniature motors directly placed at the joints solve the cable transmissions inherent issues. Unfortunately small powerfull motors are rare. As a result, these systems are rather bulky, complex and have been reported subject to early failure [9].

This paper describes an embodiment of a novel multi-arm instrument designed for the purpose of fetal spina bifida surgery. The complexity of this procedure and the governing space constraints in the uterus necessitate a small and agile robot to an extent that was not found in the literature. The paper is organized as follows : Section I.B deals with the clinical need for smaller and more performant multi-arm instruments as well as the associated technical requirements. Section II details the design of the novel instrument. Section III presents the first prototype and its characterization. Finally, Section IV concludes the paper with a discussion on the potential of this instrument. It also provides directions for further research.

B. Clinical need

There are several highly complex MIS procedures that have a clear need for instruments with smaller diameters, better dexterity and improved ergonomics. Amongst them is open spina bifida (OSB, Fig. 1). OSB is one of the most common birth defects, affecting 3,5:10000 births in the USA [13]. It is due to a incomplete closing of the neural tube and often results in severe motor and neuro-developmental impairment.

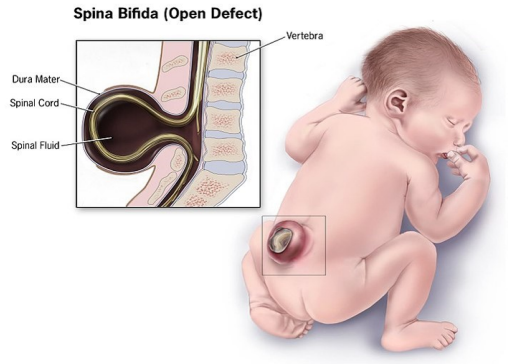

Fig. 1: Open Spina Bifida [12]

Fetal surgery has shown promising results compared to the established post-natal surgery, as earlier repair prevents potential or additional nerve damage [14]. However, open fetal surgery is associated with a high risk of preterm birth, placental abruption, maternal transfusion at delivery, pulmonary

[1]Faculty of Mechanical Engineering, Catholic University of Leuven, tom.vandebroek@kuleuven.be
[2]University Hospital Leuven
[3]School of Biomedical Engineering and Imaging Sciences, King's College London

edema or uterine dehiscence [15]. These problems arise for fetal surgery in general where - for this reason - preference is given to MIS approaches. OSB repair however is intricate and MIS approaches for this treatment are still being developed. The MIS procedure is composed of three phases. First, the fetoscopic ports are placed. Partial removal of the amniotic fluid and CO_2 insufflation is performed. The fetoscope and instruments are inserted. Second, the surgeon opens the defect and resects the extra placode that has formed above the defect. Then, the skin around the defect is separated from the muscles to stretch it above the defect. The last phase consists in suturing shut the lesion. The anatomy of the lesion may dictate the use a biosynthetic patch to protect the medula spinalis and create a watertight seal. The defect closure aims at preventing infection, protecting the previously exposed nerves and reversing brain herniation [16].

A few medical groups are pioneering this procedure. Pedrera *et al.* [15], [17] use a transcutaneous four ports technique and a biosynthetic cellulose patch. Belfort *et al.* [18] take the uterus out of the abdomen, insufflate it with CO_2 and use a two port approach for MIS with regards to the uterus. No patches or extraneous materials are used for closing the defect. Although there is no evidence yet that the above-mentioned procedures are superior to open surgery, the maternal morbidity and complications are expected to be much reduced. Uterine and placental complications such as preterm prelabor rupture of membranes and uterine dehisence however are still significant [17] .

J. Deprest *et al.* studied the fetal membranes healing properties [19],[20]. They suggested that if a single small incision ($\leq 12mm$) approach were to be available, it might reduce complications. It would also allow to use standard laparoscopy ports ([3-12mm]). With a focus on OSB, this work seeks to develop such small diameter multi-arm instrument. The envisioned SPA procedure is depicted in Fig. 2. Given the demanding requirements, it is expected that this technology would have good potential for deployment in other SPA disciplines as well. A list of requirements is provided next.

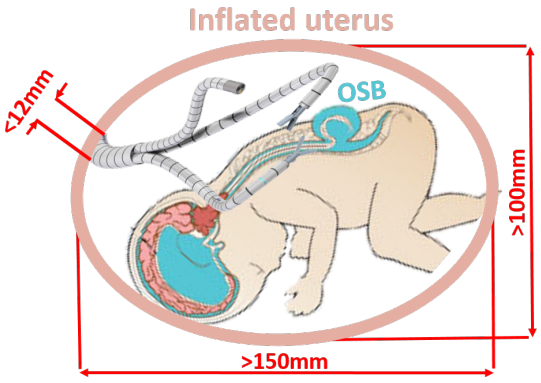

Fig. 2: Envisioned robotic procedure: a multi-arm instrument enters the uterus through a single 12mm port and repairs the OSB defect.

C. Technical requirements

General requirements for multi-arms instruments are inspired from [21] :

- **C1** Adequate maneuverability and stability
- **C2** Independent camera articulation
- **C3** Active triangulation
- **C4** Intuitive control
- **C5** Sufficiently small and interchangeable instruments
- **C6** Incorporation of an inflation/irrigation channel.
- **C7** Possibility of single-surgeon surgery

Although these characteristics are generic and need to be quantified depending on the case, no system currently satisfies all of them according to Arkenbout *et al.*[21]. Specific requirements for OSB repair include :

- **R1** *Instrument length*: the length of the deployed instruments in the uterus should not exceed 150mm as for early interventions around the 20th week of gestation, the minimum size of an CO_2 inflated uterus can be approximated an ellipsoid of $150x100x100mm$.
- **R2** *End-effector force*: the instrument should provide sufficient force for tissue manipulation and suturing. An experiment allowed to measure suturing forces between [0.5-1N]. The end-effector should therefore be able to withstand at least 1N. The experiment is described in Section III.E.
- **R3** *Interchangeable instruments*: tue to the multiple phases of the procedure, a variety of instruments is necessary. Each instrumented arm should therefore have a working channel with a minimum of 1mm inner diameter (ID) that allows interchangeability.
- **R4** The total *OD of the instrument* should be 12mm or less to minimize uterine damage according to our expert surgeons. It would also allow the use of regular laparoscopic ports. Within these 12mm there must be room for at least four working channels. Two are for the above-mentioned instruments, the third to pass a camera through and the fourth for irrigation/insufflation.
- **R5** *End-effector bandwidth*: Most instruments presented in the literature lack responsiveness. Voluntary motion goes up to 2Hz [22]. A system capable of smooth motion above 2Hz would therefore offer uncompromised maneuverability.
- **R6** *Precision*: The triangulation platform should offer a stiff and stable base for surgical precision. The combination of the end-effector precision and vibration of the platform should be smaller than human hand tremor. Coulson *et al.* [23] identified the amplitude of hand tremor to be $1.9 \pm 0.9mm$. Taking the conservative requirement of a precision $\leq 1mm$ will make sure the instrument is well-suited for complex tasks such as suturing.
- **R7** *Workspace*: The defect on the back on the baby has an ellipsoid volume with an average of $40x30x25mm$ for the semi-major/minor axes and the depth as estimated by our surgeon partners. This flattens to an ellipse of $40x30mm$ after the first incision as

the cerebral spinal fluid drains out. This forms the minimum required reachable workspace.

R8 *Triangulation*: In order for the instruments to be in a cooperative state, the angle between the end-effectors γ must be between 90° and 180° [24]. This angle is shown on Fig. 3.

Table I summarizes the functional requirements and already shows the prototype results described in Section III.

TABLE I: Functional requirements - Summary

Design parameters	Required	Achieved
R1 Deployment instrument length	$\leq$ 150 mm	135mm
R2 End-effector force	$>$ 1*N*	<1N
R3.a Instrument interchangeability	$\geq$ 1mm ID channel	OK
R4.a OD of instrument	$\leq$ 12mm	11mm
R4.b Number of channels	4	4
R5 End-effector bandwidth	$\geq$ 2Hz	2.06Hz
R6 Precision of end-effector	$\leq$ 1mm	0.75mm
R7 Task Workspace	$\geq 40\times30\times25$mm	$75\times65\times50$
R8 Triangulation angle	$90° \leq \gamma \leq 180°$	$40° \leq \gamma \leq 320°$

D. Backbone and actuation principles

Given the strategic importance of the choice in actuation and backbone for this concept, this subsection reviews some common options available for continuum robots. Table II presents the strengths and weaknesses of commonly found backbones while Table III overviews actuation principles.

TABLE II: Overview of common backbone structures with their associated strengths and weaknesses

	Strengths	Weaknesses
Spring backbone [25]	Freedom of design, simplicity, robustness, acute bending	Trade-off stiffness vs. workspace
Concentric tubes [29][30]	Small footprint, robustness, natural working channel	Friction, unstable, difficult control, bulky drive unit
Discrete serial segment [26]	Large workspace, simple model	Discrete, complex difficult manufacturing

All of these structures and actuators have their place for specific scenarios but they also present important weaknesses. The envisioned solution for fetal surgery combines multiple backbone and actuation concepts. The objective is to exploit the best of what some concepts have to offer while excluding undesired characteristics. A macro-micro approach is followed to decouple the deployment (macro) motion from the acute and dynamic distal (micro) motion.

II. System Design

A. Macro-Micro approach

Figure 3 provides a conceptual sketch of the new Macro-Micro instrument. It is composed of an insertion sheath of 11mm OD with four workings channels; two mirrored instrument arms are deployed outwards and a camera arm

TABLE III: Overview of common backbone structures with associated strengths and weaknesses

	Strengths	Weaknesses
Cable-driven actuation [6]	Standardized, cheap, established models	Friction, hysteresis, short lifetime
Concentric tubes	*See Table II*	*See Table II*
Shape memory alloy [27]	Flexibility, low footprint	Low bandwidth, high currents, high temperatures, highly non-linear
Magnetic actuation [28]	Safe, compactness in-situ	Large footprint, expensive difficult control
Fluidic actuation [32]	Large power/weight, high bandwidth, safe	Short lifetime, hysteresis, difficult control

that hovers above the instruments, offering a triangulation of the operating site. A fourth channel is available for suction and irrigation. The triangulation can be adapted during the deployment. The combined system can also rotate about its axis.

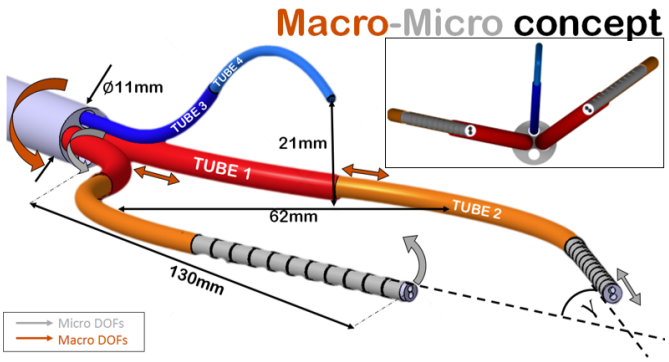

Fig. 3: Conceptual schematic of a SPA multi-arm instrument with a pair of instrument arms,a camera arm and an irrigation/suction channel

Each arm is currently envisioned to have three DOFs plus potential extra instrument DOFs as shown on Fig. 3. The instrument DOFs include opening/closing of the jaw of forceps/needle drivers and translation along the end-effector axis.

B. Macro triangulation platform

The macro part is a concentric tube robot (CTR)[29][30] forming a stable triangulation platform. The triangulation is obtained by having tube 1 diverge from the instrument axis and tube 2 converge back towards the center. The achievable curvature depends on the maximum strain of the tube. Each arm is equipped with a working channel that can fit instruments such as forceps, monopolar cautery electrode, needle drivers, etc. The modular setup allows to exchange instruments during the procedure without need of retracting the entire system. This working channel must fit side-by-side with an inflated McKibben muscle in the inner tube. The inner tube ID must therefore be $\geq 2.6mm$. The tubes parameters were selected

based on geometrical constraints and to obtain a "Dominant Stiffness Tube Pair" [30] of CTR. A stiffness ratio ≥ 3 was chosen between the tube pairs. This guarantees that the inner tube will only slightly deform the outer tube when it is inserted through it and maintain a wide triangulation. The derived parameters are presented in Table IV.

TABLE IV: Concentric tube parameters

Tube	OD/ID [mm]	Arc length [mm]	κ [mm^{-1}]	arc angle
1	4.3/3.7	56.3	0.014	45°
2	3.5/3.16	66.5	0.017	65°
3	2.3/2	30.1	0.026	45°
4	1.8/1.58	39.3	0.033	75°

Typical actuation for CTR includes translation and rotation for each tube. This yields complex and large actuation units [31]. A first key insight of the proposed triangulation platform is that it only uses translation to deploy and retract the tubes. A second key insight is that each arm rotates as one; there is no relative rotation between the concentric tubes. By mechanically constraining rotation between tubes torsional instability and snapping can be avoided. Above all, these choices simplify and significantly reduce the footprint of the drive system compared to typical CTR.

C. Micro end-effector

The micro part is a highly flexible bending segment at the tip of the macro deployment. This bending segment is actuated by a miniaturized fluidic McKibben muscle of 1.2mm OD. McKibben muscles are artificial muscles made of an elastic bladder and a rigid mesh surrounding it. When inflating the bladder, the mesh tries to maintain a constant volume. This forces the bladder expands radially and results in longitudinal contraction. In the end-effector, the muscle is attached at the tip of the segment to create a bending moment. Figure 4 provides a cross-section view of the inside of the tube, showing the working channel and the muscle.

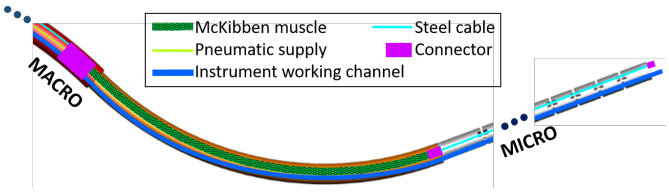

Fig. 4: Cross section view of the inner tube

Flexible backbones always are a trade-off between stiffness and range of motion (ROM). In order to overcome this trade-off, the end-effector is designed to present an anisotropic stiffness. The first direction is designed to be stiff for tissue manipulation while the second direction (perpendicular to the first) is compliant, offering a wide ROM. The bending segment is a pattern-cut NiTi tube, similar to [32]. Each segment bends up to 14°. With ten segments, the total maximum bending angle of the segment is 140°. Note that this particular pattern was used because the segment was available at the time for proof of concept. This geometry will require optimization in later work. These parameters give a range of 40°(macro deployment) to 320°(maximum micro bending) for the triangulation angle γ. This results in cooperative states between 90°-180° and 270°-320°.

This micro combination of backbone and actuator provides a high dexterity and large bandwidth. Additionally, fluidic actuation allows to truly decouple the proximal and the distal actuation: the fluidic supply lines hardly cause any parasitic motions on the macro part nor do they influence its stiffness as cables would. In cable transmission, actuating the end segments tensions the cables which go through the first segments. This modifies their stiffness and potentially displaces them unwillingly [21].

D. Camera arm

The purpose of the camera arm is to deploy above the surgical site and to offer a clear view over the combined pair of instrument arms and the targeted surgical site. It is also a CTR, the parameters of tube 3 and 4 are presented in Table IV. A $1x1mm$ chip-on-tip camera (*NanEye module F4 FOV*120°, *Awaiba*) that provides real-time vision is placed at the distal tip. The camera and tube curvatures were selected to ensure a field of view (FOV) centered on the workspace and covers both end-effectors in all configuration. The FOV is looking downwards by a standard 30° angle. The elevation, distance to target and viewing angle can be adjusted through relative tube translation.

III. First prototype & Characterisation

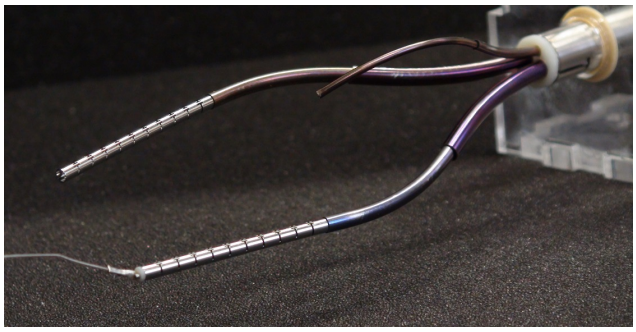

Fig. 5: View upon the first prototype of the 11mm single-port access multi-arm.

Figure 5 provides a view upon the first prototype that was built as a proof of concept. Only the micro DOFs are available for the moment as the actuation unit to deploy the different arms is still under construction. The arms are therefore manually deployed. The camera is embedded in its arm and operational. In order to validate the concept, a few experiments have been devised to characterize the system and its components.

A. Structure

The axial length of the triangulation platform plus end-effector is 135mm and the arms are deployed 46mm apart . This is in accordance with **R1**. The prototype is longer and narrower than the initial design due to the fact that the NiTi tubes always have some spring-back coming out of the mold.

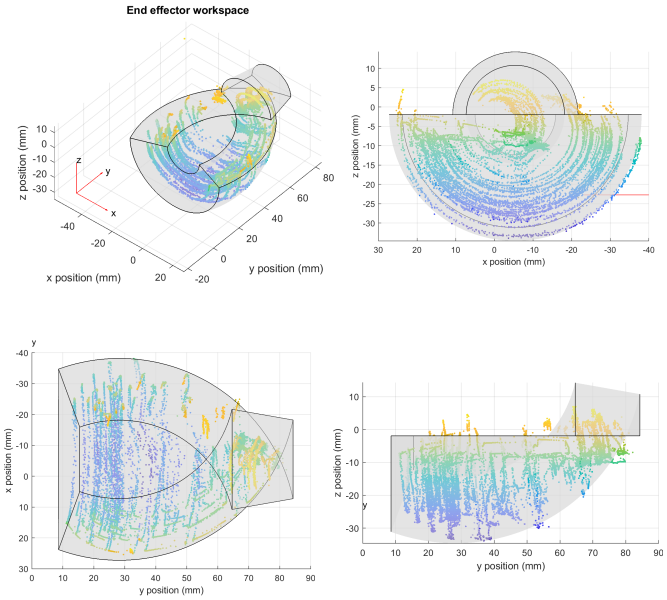

Fig. 6: Four view of the micro workspace showing the superposition of the computed and the measured workspace

The OD of the outer sheath is 11mm, respecting **R4.a**. The four working channels satisfy **R4.b**. Each arm can have a 1mm instrument inserted and retracted easily, respecting **R3**.

B. Micro Workspace

The workspace of the micro DOFs was first analytically computed based on the hypothesis that the bending segment keeps a constant curvature. It was then confirmed using an electromagnetic (EM) sensor placed at the tip of one of the arms. The Aurora system (*NDI Medical, Canada*) was used to track its position while the arm moved around its workspace. The tip of the end-effectors can bend beyond 90°, each individual arm can rotate about its base axis for about 180°. The 1mm forceps and 1mm electrode from *Karl Storz, Germany* can be translated for 20mm at the tip of the end-effector through their working channel; they start becoming too compliant further than this. The results are displayed on Fig. 6. The shell represents the analytical workspace while the cloud point was obtained with the EM tracking. The two volumes were manually aligned. It can be observed that the workspace approaches a semi-ellipsoid of $75 \times 65 \times 50$, almost twice the volume of the required $40 \times 30 \times 25mm$ defined in **R7**.

C. Dynamic behavior

In order to establish the bandwidth of our fluidic actuator, a number of pressures cycles from 0 to 4 bars have been applied to the distal actuation at increasing frequencies. A SMC ITV-0050 servovalve controls the muscle pressure. The valve has an accuracy of 0.01bar and a response time of 0.1s. White circular markers were placed at the base and the tip of the instrument to visually track its motion at 240 frame per seconds (fps). The experiment took place in a room at 35°C, approaching internal body temperature. The markers are identified in MATLAB (*Mathworks, USA*) using the *imfindcircles* function as shown in Fig. 7. The 2D coordinates of the markers are then extracted and the orientation and position of the two marker pairs are computed. This method accuracy has been evaluated on a micrometric calibration stage to be approximately 45μmm.

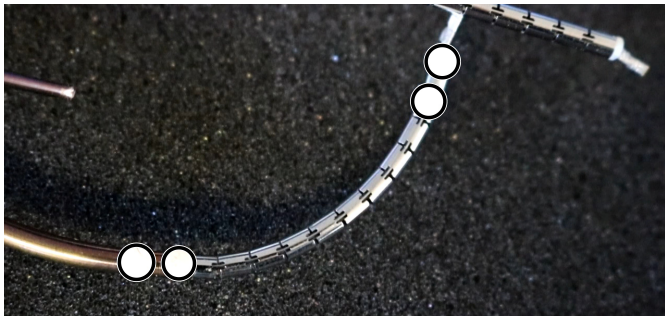

Fig. 7: Markers for image tracking on end-effector

Figure 8 presents the bending angle reached by the end-effector when excited at frequencies between [0.5-5Hz] by a sawtooth pressure signal. The angle lies at about 175° at rest and bends towards 60°. The input triangular signal is plotted as a reference in red. The upper and lower angle limits reached are marked by a red-dashed line.

The reachable range decreases as the frequency increases due to three factors. First, the 100ms response time of the valves has a large influence. Second, at higher speeds the McKibben muscle does not have time to inflate nor deflate fully. Finally, there is a time lag introduced by the supply line, experimentally found to be around 20ms for 500mm in previous work [32]. Drawing a Bode plot allows use to estimate the -3dB limit at 2.06Hz. Despite a total lag of more than 100ms from the valves and supply lines, the fluidic actuation satisfies **R5**. More performant valves would allow to increase the bandwidth even further.

As can be seen on Fig. 8, the curves are highly repeatable hence the precision of the end-effector is found acceptable as shown further in Section III.F. Table V summarizes the mean bending angle and standard deviation (STD) achieved.

TABLE V: Mean bending range & Standard deviation

	0.5Hz	**1Hz**	**2Hz**	**3Hz**	**4Hz**	**5Hz**
Mean [deg]	109.13	104.46	79.58	56.27	41.27	29.92
STD [deg]	±0.75	±1.74	±0.56	±0.46	±1.53	±1.72

D. Hysteresis

Figure 9(a) shows the hysteretic behavior of the end-effector when actuated at 0.5Hz. The red line marks the pressure dead band of 1 bar. Indeed, the McKibben muscle does not start to contract before about 1 bar, resulting in an absence of motion in that range. Therefore, the valves should never output less than 1 bar.

Figure 9(b) presents the hysteretic behaviour at the tested frequencies. Each curve was obtained by averaging 10 sample

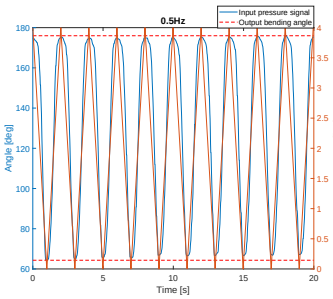

(a) 0.5Hz - A = 111.65°

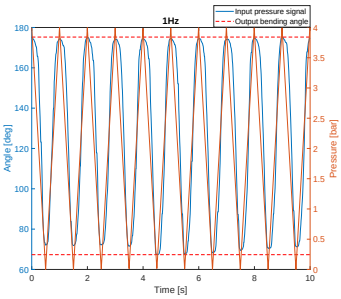

(b) 1Hz - A = 107.93°

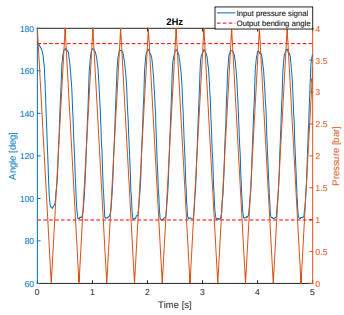

(c) 2Hz - A = 80.54°

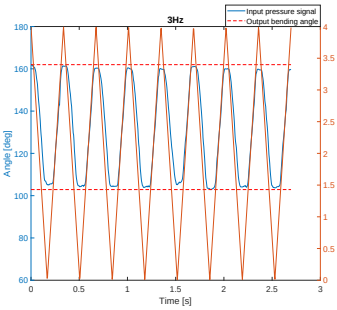

(d) 3Hz - A = 59.08°

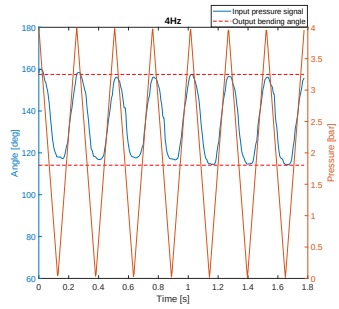

(e) 4Hz - A = 45.75°

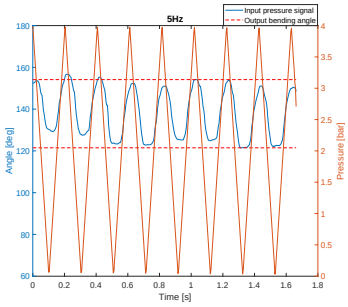

(f) 5Hz - A = 36°

Fig. 8: Dynamic behavior of end-effector (Frequency - Amplitude)

curves as shown on Fig. 9(a). To evaluate the importance of the hysteresis, each curve was regressed linearly and the divergence between the ideal linear behavior and the hysteresis was evaluated in Table VI.

TABLE VI: End-effector bending hysteresis linear divergence

	0.5Hz	1Hz	2Hz	3Hz	4Hz	5Hz
Mean divergence [deg]	12.46	11.92	6.95	5.49	4.62	4.56
Max divergence [deg]	30.10	28.12	15.34	13.03	9.25	11.87

E. Evaluation of the strength and force of the end-effector

It is important that the end effector can withstand sufficient forces for tissue manipulation and suturing. A needle holder and a Nano25 6DOFs sensor from *ATI, USA* were interfaced. A needle was placed at the tip and a suture motion was performed repetitively though a chicken thigh skin and muscle. The first half were done from inside of the incision piercing muscle

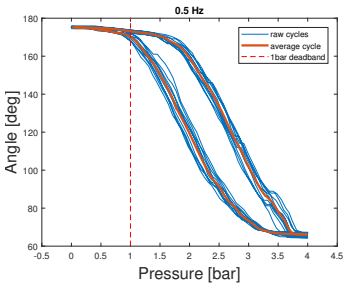

(a) 0.5Hz

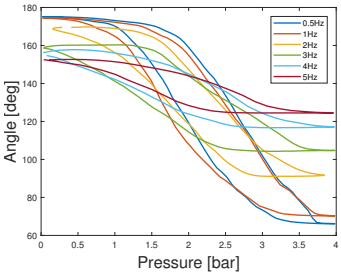

(b) 0.5Hz-5Hz

Fig. 9: End-effector hysteresis

then skin; the second half from the outside, piercing skin then muscle. As can be seen of Fig. 10 most sutures required less than 1N, the largest peak reaching 1.2N. Given that chicken skin is thicker than a fetus skin, one can safely assume that 1N will be sufficient as posed in **R2**.

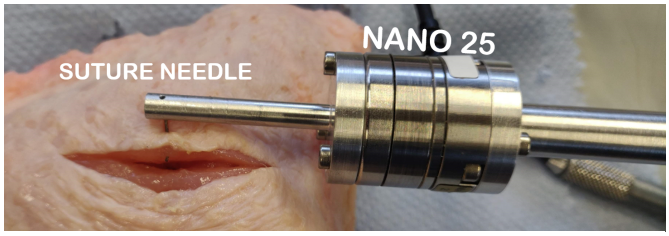

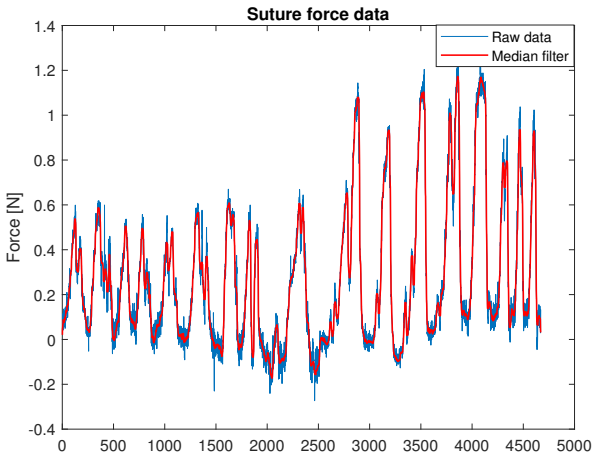

Fig. 10: Suture force measurement

Transversal strength: the strength in the transversal directions to the bending was first evaluated suspending a 1N weight at the tip and bending the segment. The segment support the 1N weight until about a 45° bending but then collapses. The reason for this behaviour can be understood from observing the NiTi stress-strain curve. The NiTi presents two elastic domains as detailed in [33]. First, the material goes through a linear elastic domain up to a first yield point with a strain of about $1-1.5\%$ and a high Young modulus ([41-83 GPa]). This yield point can be found between 195 and 690MPa, depending on the alloy composition and quality. Passed this point, the material goes through a superelastic plateau, up to a strain of $8-11\%$ with only a small increase

in stress. Such a large deformation is not desired in the transversal direction therefore the stress should not exceed the yield point and remain in the linear elastic region (austenitic state). **R2** is therefore not respected and optimizing the end-segment by tuning the tube thickness, tube length and cut-out pattern will be necessary in the next iteration.

Bending force: the force in the direction of bending was evaluated by lifting various weights with the end-effectors, departing from a straight to a contracted position as shown on Fig. 11. The minimum pressure required was noted when the arm could not hold the weight anymore and collapsed. The results are presented in table VII according to the weight lifted and the corresponding operational pressure range. Above 0.08N, the arm could hold the weight at high pressure but was not able to lift it back up after relaxing.

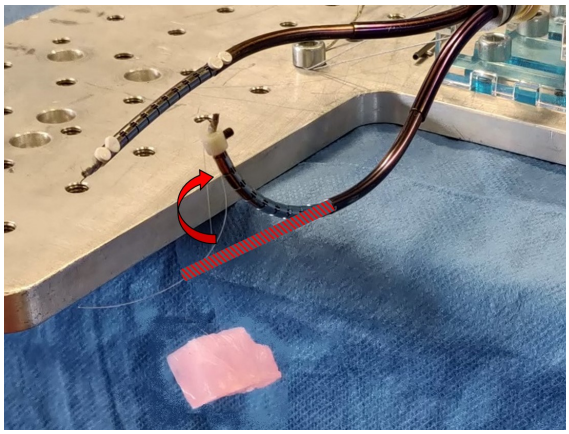

Fig. 11: Force characterization setup

TABLE VII: Bending strength

Lifted weight [N]	0.02	0.03	0.04	0.05	0.06	0.07	0.08
Min. pressure [bar]	2	2	2	2.3	2.6	3	3.3

The end-effector bending is used to attain a desired position while remaining compliant. Tasks requiring force like lifting tissue or suturing are expected to be done by rotating the arm outwards, using the transversal rigidity. However, the results of Table VII are smaller than the expected values. This can be explained by the length of the McKibben muscles used. Indeed, the static force they display quickly drops as they contract during the bending motion [34]. Therefore, a longer muscle would contract less relatively and maintain a higher force. Another solution to increase the strength of the segment would be to move the muscle anchor closer to the edge of the end-effector tip. The lever, and hence the moment, could be doubled by optimizing the anchor position. These two proposed corrections would multiply the lifting force and will be implemented in the next iteration.

F. Stability of the triangulation & end-effector precision

The stability of the CTR platform has been evaluated during the dynamic experiment (Subsection III.C) using a fusionTrack 250 optical tracker (*Astracsys, Switzerland*. A reflective marker was placed near the junction of the two tubes as shown in Fig. 12. First a static sample was taken as a reference to evaluate the noise and drift of the sensor. The noise was found to be contained within $\pm 10\mu m$ and a slow drift was identified. The results were therefore de-trended in Matlab to cancel the drift. Fig. 13 shows the vibration response of the deployment platform to the end-effector motion for 0.5Hz and 1Hz excitations. The response is in phase with the excitation and its amplitude ranges from $72\mu m$ at 0.5Hz to $16\mu m$ at 5Hz.

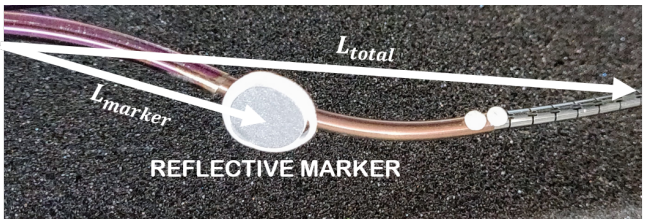

Fig. 12: Optical marker

The measured vibration is amplified at the tip by a factor of $L_{total}/L_{marker} = 2.7$ due to the marker placement (see Fig. 12). To establish the minimum precision of the end-effector tip, one must first convert the angular STD obtained in Table V to a translational STD. The tip of the bending segment follows an arc of radius $r_b = 37.4mm$. A 1° precision therefore corresponds to 0.65mm. By summing the vibration amplitude and the STD, the precision is obtained and presented in table VIII. The average obtained precision is 0.75mm $<$ 1mm, respecting **R6**. It can be noted that the main influence comes from the bending precision.

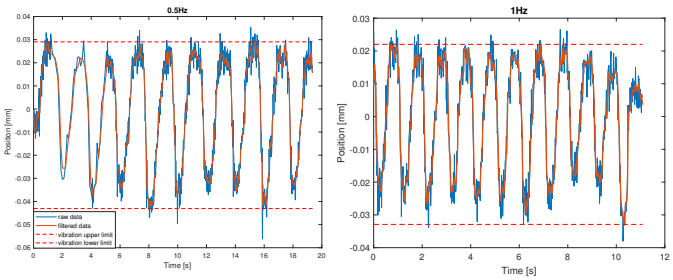

(a) 0.5Hz - 72μm (b) 1Hz - 55μm

Fig. 13: Stability of the triangulation platform (Excitation frequency - vibration amplitude)

TABLE VIII: Precision of the end-effector

	0.5Hz	**1Hz**	**2Hz**	**3Hz**	**4Hz**	**5Hz**
Bending STD ±[mm]	0.49	1.13	0.36	0.3	0.99	1.12
Vibration ±[mm]	0.04	0.03	0.02	0.01	0.01	0.01
Precision [mm]	0.53	1.16	0.38	0.31	1.00	1.13

IV. Conclusion

In this paper a new concept of a multi-arm instrument for SPA surgery was presented. All the functional require-

ments were respected. The instrument possesses many of the ideal characteristics mentioned in section I.B as stability, independent camera articulation, active triangulation, small and interchangeable instruments. It is however too early to evaluate maneuverability as not all DOFs are available yet. The specific requirements and the prototype characterization are summarized in Table I. All requirements are respected except for **R2**. To attain **R2** over the whole ROM, the bending end-effector will be re-designed for the next iteration.

The instrument offers a considerably lower diameter than the state of the art instruments. Table IX summarizes the main multi-arm robotic SPA platforms and their diameters. According to [21] and to the best knowledge of the authors, this paper proposes the first multi-arm instrument with a hybrid actuation combining intrinsic and extrinsic approaches. A smooth and dynamic behavior is obtained thanks to the macro-micro decoupling and to the fluidic actuation. It was show experimentally that the distal actuation can move precisely and dynamically without affecting the stability of the triangulation.

TABLE IX: Outer diameter of state of the art multi-arm instruments

Reference	**OD**	**Reference**	**OD**
da Vinci SP [35]	25mm	SPORT [*TITAN medical*]	20mm
Lau et al. [7]	18mm	SPRINT [10]	18mm
IREP [6]	15mm	SAIT [8]	20mm
MASTER [4]	22mm	Lehman et al. [11]	26mm
STRAS [3]	16mm	**Macro-Micro multi-arm**	**11mm**

There is still some work ahead to build an actuation system to translate the individual triangulating arms. A major challenge will consist in developing a compact drive system to steer the many DOFs in an intuitive manner. While we are interested to understand what are the least amount of DOFs to conduct a task efficiently, such information can only come from user experiments. Further work will therefore focus in investigating experimentally what DOFs are essential.

ACKNOWLEDGMENT

This work was supported through an Innovative Engineering for Health award by Wellcome Trust [WT101957]; Engineering and Physical Sciences Reserach Council (EPSRC) [NS/A000027/1] and through a personal Strategic-Basic research Fellowship of the Research Foundation - Flanders (1S96518N).

REFERENCES

[1] Pignata, Giusto ; Corcione, Francesco ; Bracale, Umberto. Single-Access Laparoscopic Surgery. Cham: Springer International Publishing, 2014.
[2] Supe, A. et al (2010). Ergonomics in laparoscopic surgery. Journal of Minimal Access Surgery, 6(2), 316.
[3] De Donno, A. et al. (2013). Introducing STRAS: A new flexible robotic system for minimally invasive surgery. IEEE ICRA, 1213-1220.
[4] Phee SJ et al. (2009) Master and slave robot for natural orifice translumenal endoscopic surgery. Conf Proc IEEE Eng Med Biol Soc ;4:1192e5.
[5] Abbott,D. et al. (2007). Design of an endoluminal NOTES robotic system. IEEE IROS, 410-416.
[6] Ding et al. (2013). Design and coordination kinematics of an insertable robotic effectors platform for single-port access surgery. IEEE/ASME Transactions on Mechatronics, 18(5), 16121624.
[7] Lau et al. (2016). A Flexible Surgical Robotic System for Removal of Early-Stage Gastrointestinal Cancers. IEEE TII.
[8] Roh et al. (2015). Development of the SAIT robot slave arm based on RCM Mechanism. Proceedings of IEEE EMBS, 52855290.
[9] Yeung, B et al. (2012). A technical review of flexible endoscopic multitasking platforms. International Journal of Surgery, 10(7), 345354.
[10] Petroni et al. (2013). A novel intracorporeal assembling robotic system for single-port laparoscopic surgery. Surg. Endo. and Other Interv. Techniques, 27(2)
[11] Lehman et al. (2011). Dexterous miniature robot for advanced minimally invasive surgery. SSurg. Endo. and Other Interv. Techniques, 25(1)
[12] Public domain, Centers for Disease Control and Prevention, United States Department of Health and Human Services
[13] CDC, Notes from the field (2013): investigation of a cluster of neural tube defects Washington. MMWR Morb Mortal Wkly Rep; 62: 728.
[14] Anon,(2003). Prenatal Surgery; Fetal surgery for spina bifida shows benefits in leg function, fewer shunts. Health & Medicine Week, p.608.
[15] Mazzone, L., and M. Meuli. Re: Fetoscopic Repair of Spina Bifida: Safer and Better? Ultrasound in Obstetrics &Amp; Gynecology, vol. 48, no. 6, 2016, p. 802.
[16] Scott Adzick, N. (2012). Fetal Surgery for Spina Bifida: Past, Present, Future. Seminars in Pediatric Surgery, Seminars in Pediatric Surgery
[17] Pedreira, D. A. L., et al. Fetoscopic Repair of Spina Bifida: Safer and Better? Ultrasound in Obstetrics &Amp; Gynecology, vol. 48, no. 2, 2016, pp. 141147.
[18] Belfort, A et al (2017). Fetoscopic Open Neural Tube Defect Repair: Development and Refinement of a Two-Port, Carbon Dioxide Insufflation Technique. Obstetrics & Gynecology, 129(4), 734-743.
[19] Gratacs E., Sanin-Blair J., Lewi L., Toran N., Verbist G., Cabero L., Deprest J. (2006). A histological study of fetoscopic membrane defects to document membrane healing. Placenta, 27 (4-5), 452-6.
[20] Devlieger R., Gratacs E., Wu J., Verbist L., Pijnenborg R., Deprest J. (2000). An organ-culture for in vitro evaluation of fetal membrane healing capacity. European Journal of Obstetrics & Gynecology and Reproductive Biology, 92 (1), 145-50.
[21] Arkenbout, E. A. et al. (2015). A state of the art review and categorization of multi-branched instruments for NOTES and SILS. Surgical Endoscopy and Other Interventional Techniques, 29(6), 12811296.
[22] Riviere, C. et al. (1997). Characteristics of hand motion of eye surgeons. Proceedings International Conference of the IEEE EBMS, 4, 1690-1693.
[23] Coulson et al. (2010). The effect of supporting a surgeons wrist on their hand tremor. Microsurgery, 30(7), 565568.
[24] M. T. Chikhaoui et al. (2018). Toward Motion Coordination Control and Design Optimization for Dual-Arm Concentric Tube Continuum Robots. IEEE RAL, vol. 3, no. 3, pp. 1793-1800.
[25] Kutzer, M. et al. (2011). Design of a new cable-driven manipulator with a large open lumen: Preliminary applications. ICRA, , 2913-2920.
[26] K.-W. Kwok et al. (2013). Dimensionality reduction in controlling articulated snake robot for endoscopy under dynamic active constraints. IEEE Trans. Robot.,vol. 29, no. 1, pp. 15-31.
[27] P. Dario et al.(1997) A miniature steerable end-effector for application in an integrated system for computer-assisted arthroscopy. ICRA proc.
[28] Di Natali et al. (2015). Surgical robotic manipulator based on local magnetic actuation. Journal of Medical Devices, 9(3), 030936.
[29] Webster, R., Romano, J., Cowan, N. (2009). Mechanics of Precurved-Tube Continuum Robots. Robotics, IEEE Transactions on, 25(1), 67-78.
[30] Dupont et al. (2010). Design and Control of Concentric-Tube Robots. Robotics, IEEE Transactions on, 26(2), 209-225.
[31] Mahoney, A. W (2016). A Review of Concentric Tube Robots: Modeling, Control, Design, Planning, and Sensing. Encyclopedia of Medical Robotics, 122.
[32] Devreker et al. (2015) Fluidic actuation for intra-operative in situ imaging. IEEE/RSJ IROS 2015 pp. 1415-1421.
[33] Lagoudas, D. (2008). Shape Memory Alloys: Modeling and Engineering Applications. Boston, MA: Springer US.
[34] De Volder et al. (2011). Fabrication and control of miniature McKibben actuators. Sensors and Actuators A: Physical, 166(1), 111-116.
[35] Tsang et al.(2016). Transoral endoscopic nasopharyngectomy with a flexible robotic surgical system. Laryngoscope, 126(10), 22572262